

Ground State Properties of the Doped 3-Leg t - J Ladder

Steven R. White¹ and D.J. Scalapino²

¹*Department of Physics and Astronomy, University of California, Irvine, CA 92697*

²*Department of Physics, University of California, Santa Barbara, CA 93106*

(September 17, 2018)

Abstract

Results for a doped 3-leg t - J ladder obtained using the density matrix renormalization group are reported. At low hole doping, the holes form a dilute gas with a uniform density. The momentum occupation of the odd band shows a sharp decrease at a large value of k_F similar to the behavior of a lightly doped t - J chain, while the even modes appear gapped. The spin-spin correlations decay as a power law consistent with the absence of a spin gap, but the pair field correlations are negligible. At larger doping we find evidence for a spin gap and as x increases further we find 3-hole diagonal domain walls. In this regime there are pair field correlations and the internal pair orbital has $d_{x^2-y^2}$ -like symmetry. However, the pair field correlations appear to fall exponentially at large distances.

PACS Numbers: 74.20.Mn, 71.10.Fd, 71.10.Pm

I. INTRODUCTION

The recently discovered n -leg ladder cuprate materials [1] form an interesting testing ground for ideas regarding strongly correlated electron systems. Just as for the two-dimensional layered cuprates, the t - J Hamiltonian is believed to provide a basic model which contains the general features of the ladder systems. In particular, the undoped, even-leg Heisenberg ladders have been shown to exhibit a spin gap [2,3], while the odd-leg ladders have no spin gap, in agreement with experiment [4]. Various calculations on the doped 2-leg ladder find that in the ground state the doped holes form $d_{x^2-y^2}$ -like pairs, and the system is characterized by power-law pair-field and $4k_F$ -CDW correlations [5–7]. A recent study of the 4-leg doped t - J model [8] found evidence for three types of phases, depending upon the ratio of J/t and the hole doping x . At low doping, when holes are first added to the insulating state, they form a dilute gas of $d_{x^2-y^2}$ -like pairs. At higher doping, the holes arrange themselves into fluctuating domain walls while maintaining significant $d_{x^2-y^2}$ pair-field correlations. Finally, at sufficiently large J/t values ($\gtrsim 1.5$), phase separation occurs. Based upon these results, it is interesting to explore what happens when an odd-leg ladder is doped. Here we discuss results obtained from density matrix renormalization group (DMRG) calculations [9,10] for a doped 3-leg t - J ladder.

The t - J Hamiltonian which we will study has the form

$$\mathcal{H} = J \sum_{\langle ij \rangle} \left(\vec{S}_i \cdot \vec{S}_j - \frac{1}{4} n_i n_j \right) - t \sum_{\langle ij \rangle, s} P_G \left(c_{i,s}^\dagger c_{j,s} + c_{j,s}^\dagger c_{i,s} \right) P_G. \quad (1)$$

Here $\langle ij \rangle$ denotes nearest-neighbor sites on the ladder, s is a spin index, \vec{S}_i and $c_{i,s}^\dagger$ are electron spin and creation operators, $n_i = c_{i,\uparrow}^\dagger c_{i,\uparrow} + c_{i,\downarrow}^\dagger c_{i,\downarrow}$ and the Gutzwiller projector P_G excludes configurations with doubly occupied sites. For the DMRG calculations discussed here we have used open boundary conditions for $L \times 3$ clusters and have set $J/t = 0.35$, which is close to the value expected for the cuprates. From 800 to 1500 states were kept per block. Truncation errors were typically $\sim 10^{-5}$.

In the next section, II, we begin by showing the most probable ground state hole con-

figurations and the over-all structure of the charge and spin correlations for different hole densities. While these projections show only a caricature of the groundstate which contains a huge superposition of states corresponding to large fluctuations of the structures shown, they provide a useful picture for the discussion which follows. In particular, the average hole rung density shows that the domain wall structure seen in the projections can survive in a ground state expectation value.

In Section III, we calculate the momentum distribution of the holes and use it to discuss the nature of the quasiparticle excitation bands. Following this, in Section IV, we examine spin correlation and the behavior of the spin gap in the doped system. In Section V we discuss the orbital structure of the pairs and the pairing correlations. Section VI contains our conclusions.

II. CHARGE DENSITY AND SPIN STRUCTURE

As we have previously discussed [11], two holes doped into a 3-leg t - J ladder are not bound for physically relevant values of J/t . However, we have found that as holes are added at a fixed value of J/t , the system evolves from a gas of holes to an array of domain walls as shown in Fig. 1. This figure shows the most probable configuration of holes in the system for $J/t = 0.35$ obtained by maximizing the ground state expectation value of

$$P(\ell_1, \ell_2, \dots) = \prod_{i=1} p(\ell_i), \quad (2)$$

with $p(\ell_i) = (1 - n_{\ell\uparrow})(1 - n_{\ell\downarrow})$ the hole projection operator for the ℓ^{th} lattice site. Here $(\ell_1, \dots, \ell_{N-1})$ are chosen to give the most probable location of $N - 1$ holes, and for this configuration, the diameter of the dark circles gives the probability of finding the N^{th} hole on a given site.

At low hole concentrations, the most likely configuration consists of individual holes as shown in Fig. 1(a). The most probable location for the holes are on the outer legs and as we will see reflect the fact that in the dilute limit the holes are doped into the odd single particle

band. As the density x of holes increases, fluctuating domain wall-like arrays appear. This initially occurs as a domain wall running down the center chain as seen in Fig. 1(b). At higher densities, fluctuating diagonal three-hole domain walls appear as shown in Fig. 1(c).

The local structure of these diagonal domain walls is similar to that of the diagonal domain walls observed on 4-leg ladders [8]. Figure 2 shows a section of the lattice which contains a three-hole domain wall. Figure 2(a) shows the strength of the exchange field $-\langle \vec{S}_i \cdot \vec{S}_j \rangle$ when the holes occupy their most likely positions. The strong diagonal singlet correlations in Fig. 2(a) are similar to those which are found for $d_{x^2-y^2}$ -pairs on the even leg ladders as well as on 2D lattices. These diagonal singlet correlations reflect the fluctuating nature of the wall which reduces the kinetic energy of localization, while at the same time minimizing the exchange energy. In Fig. 2(b), an external staggered magnetic field has been applied to the left-hand end of the ladder, and one can see that the antiferromagnetic spin background undergoes a π -phase shift as it crosses the domain wall.

Another view of this is given in Fig. 3(a) which shows the average charge density and the spin structure. Here, as in Fig. 2(b), a small staggered magnetic field has been applied to the left hand end. Fig. 3(b) shows a view of the longitudinal domain wall of Fig. 1(b). Here there is a small staggered field along the bottom leg. The resulting spin moments on the top leg are π -phase-shifted with respect to the bottom leg. The crossover from longitudinal to transverse (diagonal) domain walls appears to be smooth as x increases.

The development of transverse domain walls is also clearly evident in Fig. 4, which shows the average rung density

$$\langle n_\ell \rangle = \frac{1}{3} \sum_{j=1}^3 \langle n_{\ell j} \rangle. \quad (3)$$

The open boundary conditions break translational invariance, allowing density variations to be seen. At low hole and moderate hole densities (the lower two curves), the average rung density is fairly uniform, corresponding to individual holes and to a longitudinal domain wall. At a filling of 18 holes on a 32×3 ladder, corresponding to $x = 0.1875$, six three-hole diagonal domain walls are clearly evident in the top curve in Fig. 4.

III. MOMENTUM DISTRIBUTION OF THE HOLES

The one-electron eigen operators of a non-interacting 3-leg ladder have the structure

$$\gamma_{k_x, k_y, s}^\dagger = \sum_{\ell=1}^3 \frac{\sin k_y \ell}{\sqrt{2}} c_{k_x, \ell, s}^\dagger, \quad (4)$$

with $k_y = \pi/4, \pi/2$, and $3\pi/4$. The corresponding eigen energies are

$$\varepsilon_k = -2t(\cos k_x + \cos k_y). \quad (5)$$

The states $k_y = \pi/4$ and $3\pi/4$ are even under reflection about the center chain, while the $k_y = \pi/2$ state is odd.

Using the DMRG technique, we have calculated the equal time expectation value $\langle \psi_0 | c_{i_x, i_y, s}^\dagger c_{j_x, j_y, s} | \psi_0 \rangle$ and from this constructed the momentum occupation expectation values for the three k_y -bands

$$\langle \psi_0 | n_{k_x, k_y, s} | \psi_0 \rangle = \langle \psi_0 | \gamma_{k_x, k_y, s}^\dagger \gamma_{k_x, k_y, s} | \psi_0 \rangle. \quad (6)$$

Figure 5(a) shows the momentum occupation for the three bands at low doping, $x = 0.042$. For comparison, the momentum occupation for a single chain t - J model with $J/t = 0.35$ and a hole density $x = 0.1$ is shown in Fig. 5(b). The decrease of $n(k)$ sharpens as the length of the t - J chain is increased and marks the Fermi wave vector k_F of the single-chain Luttinger liquid. The structure of $\langle n_{k_x k_y} \rangle$ for the odd $k_y = \pi/2$ band is similar to that of the single chain t - J system. This suggests that at low doping, the $k_y = \pi/2$ band of the 3-leg system is not gapped at the Fermi surface, while the two even bands at $k_y = \pi/4$ and $3\pi/4$ appear to be gapped. When the density of holes is increased, all three bands appear to be gapped, as shown in Fig. 6(a) and (b) for $x = 0.125$ and $x = 0.1875$ respectively. These conclusions are confirmed by direct observation of $\langle \psi_0 | c_{i_x, i_y, s}^\dagger c_{j_x, j_y, s} | \psi_0 \rangle$ as a function of $i_x - j_x$ (not shown): at low densities, power law decay is observed in the odd mode, and exponential decay in the even modes, while at higher densities, all modes show exponential decay.

IV. SPIN CORRELATIONS

Based upon the quasi-particle momentum distributions discussed in Section III, we would expect that the lightly doped 3-leg ladder would exhibit power-law antiferromagnetic correlations arising from the $k_y = \pi/2$ quasi-particle band. A log-log plot of $\langle S_i^z S_j^z \rangle$ for $x = 0.042$ is shown in Fig. 7(a) and is consistent with the power law decay one would expect for a one-dimensional Luttinger liquid. At higher hole densities $x = 0.125$ and 0.1875 , the spin-spin correlations $\langle S_i^z S_j^z \rangle$ are found to decay exponentially as shown in Fig. 7(b). This is consistent with the behavior of $\langle n_k \rangle$ discussed in the previous section.

We have also calculated the spin gap

$$\Delta_S = E_0(S_z = 1) - E_0(S_z = 0) \quad (7)$$

as a function of the hole doping x for a 44×3 ladder. Here $E_0(S_z)$ is the ground state energy with a given value of total spin S_z . The result is shown in Fig. 8. We believe that the non-vanishing spin gap for $x \lesssim 0.05$ is a finite size effect and that the spin gap will extrapolate to zero in the low-doping region. At higher doping, there is a spin gap consistent with the exponential decay of the spin-spin correlations.

V. PAIRING CORRELATIONS

In order to determine the orbital structure of the pairs, we have calculated the off-diagonal expectation value

$$_{N-2} \langle \psi_0 | c_{\ell\uparrow} c_{n\downarrow} | \psi_0 \rangle_N \quad (8)$$

on a 16×3 ladder with $N = 4$ holes. The results of this calculation are shown in Fig. 9(a). Here, one member of a singlet pair is located at the site marked by the solid circle. The shaded circles indicate the amplitude and sign for finding the second member. The internal structure of the pair has a $d_{x^2-y^2}$ -like form, although it is somewhat asymmetric with an admixture of s due to the 3-leg nature of the cluster.

We have also calculated the pair field–pair field correlation function

$$D(\ell_x) = \langle \psi_0 | \Delta_{i_x + \ell_x} \Delta_{i_x}^\dagger | \psi_0 \rangle. \quad (9)$$

Here $\Delta_{i_x}^\dagger$ creates a $d_{x^2-y^2}$ -like pair around the i_x site of the middle leg,

$$\Delta_{i_x}^\dagger = c_{i_x, 2\uparrow}^\dagger (c_{i_x+1, 2\downarrow}^\dagger - c_{i_x, 3\downarrow}^\dagger + c_{i_x-1, 2\downarrow}^\dagger - c_{i_x, 1\downarrow}^\dagger) - (\uparrow \leftrightarrow \downarrow) \quad (10)$$

$D(\ell_x)$ is plotted in Fig. 9(b) for various values of the hole doping. In the regime of low doping $x \lesssim .05$, the pair field correlations are negligible. At larger values of doping x , short range pair field correlations are present. However, as shown by the semi-log plot in Fig. 9(c), these pairing correlations appear to decay exponentially at large distances.

While the pair-field correlations do not exhibit the power law decay found for a two-leg ladder, there are clearly significant short range pairing correlations as seen in Fig. 9(b). In order to examine these, we have calculated the response of the system to a proximity pairing field

$$H_1 = d \sum_i (\Delta_{i, i+\hat{y}}^\dagger + \Delta_{i, i+\hat{y}}). \quad (11)$$

Here

$$\Delta_{i, i+\hat{y}}^\dagger = c_{i, \uparrow}^\dagger c_{i+\hat{y}, \downarrow}^\dagger - c_{i, \downarrow}^\dagger c_{i+\hat{y}, \uparrow}^\dagger \quad (12)$$

adds a singlet electron pair to sites i and $i+\hat{y}$. In this case, the DMRG calculation breaks up the Hilbert space into N modulo 2 sectors, keeping total S_z as a good quantum number. The response was then determined by measuring the strength of the induced pair field in both the \hat{x} and \hat{y} directions, $\langle \Delta_{i, i+\hat{x}} \rangle$ and $\langle \Delta_{i, i+\hat{y}} \rangle$ for all sites i . The interaction H_1 couples equally to extended s -pairs and $d_{x^2-y^2}$ pairs. However, in all the cases that we have studied which show significant pairing correlations, $\langle \Delta_{i, i+\hat{x}} \rangle$ and $\langle \Delta_{i, i+\hat{y}} \rangle$ have different signs, reflecting the $d_{x^2-y^2}$ -like symmetry of the response.

In order to compare the $d_{x^2-y^2}$ response of the 3-leg ladder with that of the 2- and 4-leg ladders, we have made similar measurements on each of these ladders. Figure 10 shows a plot of the average $d_{x^2-y^2}$ pair field response

$$\langle \Delta_d \rangle = \frac{1}{N} \sum_i (\langle \Delta_{i,i+y} \rangle - \langle \Delta_{i,i+x} \rangle) \quad (13)$$

for $n = 1$ -, 2-, 3-, and 4-leg ladders versus doping x . It is clear from this result that the 3-leg ladder has a comparable $d_{x^2-y^2}$ pair field response to that of both the 2- and 4-leg ladders. This is expected from both weak coupling RPA calculations [12] and renormalization-group studies [13–15]. However, in the presence of the 3-hole striped domain wall structure shown in Figs. 1, 2, and 3, it may seem unusual. In order to understand it in the present framework, we have studied the typical hole configurations which contribute to the pair field correlations for a 12×3 ladder with 6 holes [8]. In Fig. 11(a), we show typical hole configurations in a system with two diagonal domain walls. These configurations show the large fluctuations present in the domain walls. These large fluctuations allow a significant pairing response despite the presence of the domain wall charge density wave. In Fig. 11(b), we show some of the specific hole configurations which give rise to pairing correlations. In particular, we measure

$$\langle \psi_0 | \Delta_{i,i+y} \Delta_{j,j+y}^\dagger P(\ell_1, \ell_2, \dots, \ell_{N-2}) | \psi_0 \rangle, \quad (14)$$

where P is given in Eq. (2), and N is the number of holes. Here the two shaded holes on the right indicate where a singlet pair of holes is removed and the two shaded holes on the left where a singlet pair is added. These points are kept fixed. The black points show typical locations of the remaining four holes, obtained using a Monte Carlo procedure using DMRG to measure the probability of a configuration, given by the absolute value of Eq. (14) [8]. The configurations show that groups of one, two, and three holes are common. Most often, a pair is created or destroyed next to a third hole, thus converting a domain wall into a single hole and vice-versa. From these one obtains a general idea of how pairing correlations and fluctuating domain walls coexist.

VI. CONCLUSIONS

From these DMRG results for the 3-leg t - J ladder, the following picture emerges. Initially, when a low concentration of holes is added to the 3-leg ladder, the holes form a dilute gas with a uniform density, except near the ends of the open ladder. The holes tend to occupy the outer legs, associated with the odd quasiparticle mode. The momentum occupation $\langle n_{k_x k_y} \rangle$ indicates that the $k_y = \pi/2$ odd mode is gapless, while the $k_y = \pi/4$ and $3\pi/4$ even modes are gapped. In this low doping regime, the spin-spin correlations exhibit an approximate power law decay, and we believe that the spin gap extrapolates to zero. The pairing correlations are negligible.

At higher hole densities, fluctuating domain walls appear. These walls have a similar structure to the domain walls found in previous DMRG studies. For $x = 0.125$ and 0.1875 , the change in momentum occupation $\langle n_{k_x k_y} \rangle$ is broad for all three bands, consistent with the finite spin gap observed on the 44×3 lattice for $x \gtrsim 0.06$. In this regime the spin-spin correlations decay exponentially and there are significant short-range $d_{x^2-y^2}$ -like pairing correlations.

These results have a number of similarities to other recently reported results for the 3-leg ladder. Rice, et. al. [16] have carried out Lanczos calculations on doped 8×3 clusters as well as a mean field analysis. They suggest that below a critical doping the odd band forms a Luttinger liquid and the two even bands an insulating spin liquid. Our results for the momentum occupation $\langle n_{k_x k_y} \rangle$, and the spin-spin correlations support this picture.

Renormalization group and bosonization calculations [13–15] for a 3-leg ladder suggest that the doped isotropic t - J system has a C2S1 phase with two gapless charge modes and one gapless spin mode. This is also consistent with what we have found. However, in addition to power law spin-spin correlations, and a gapless odd mode, this phase is expected to have power law pairing correlations. However, at low doping we find that pairing correlations are not present (see Fig. 9(b)). Similarly, mean field theory [16] and RPA calculations [12] suggest that the system will exhibit pairing correlations at low doping. However, it appears

from the DMRG results that a critical hole density of order $x \approx 0.06$ is required before this occurs. Rice, et. al. [16] have argued that this critical doping x_c is associated with a doping concentration at which the chemical potential becomes equal to the two hole bound state energy of the spin liquid. From small cluster Lanczos calculations they estimate $x_c \approx 0.13$, but note that it could be less, while as discussed in Sec. IV, we find an onset of a spin gap at about half this value.

At larger values of doping we indeed find measurable $d_{x^2-y^2}$ -like pair field correlations. However they appear to decay exponentially rather than as a power law. Nevertheless, other measurements, such as the “proximity” response of the 3-leg ladder indicate that significant pair correlations are present. In this same doping regime we find a spin gap and observe that the momentum occupation is broadened for all three quasi-particle modes. Except for the absence of power law pair field correlations and the prominence of the domain wall structures, this higher doping regime has a number of features similar to a Luther-Emery liquid. Rice, et. al. [16] have suggested that the system makes a transition into a Luther-Emery liquid when the doping is such that holes can enter the even-parity quasi-particle modes.

The present work also shows that there is a close relationship between the appearance of fluctuating domain wall configurations and pairing [17]. In particular, both longitudinal [Fig. 1(b)] and transverse (diagonal) [Fig. 1(c)] domain walls occur in the doping regime where the pairing correlations appear. However, in this case, these domains are not produced by a competition between phase separation and long range Coulomb interaction [17]. For 3-leg ladders, phase separation requires unphysically large values of J/t and there is no long range Coulomb interaction in our model. In the present work, the domain walls arise as a compromise to minimize the kinetic energy of the holes and the exchange energy of the spin background. The local structure of the domain walls shown in Fig. 2 exhibits hole-hole correlations and exchange bonding $\langle \vec{S}_i \cdot \vec{S}_j \rangle$ correlations similar to those associated with pairs [11]. In addition, as shown in Fig. 11, pairs can fluctuate between the domain walls. This is similar to the 4-leg ladder except that in the 3-leg ladder, the three-hole diagonal walls

contain an extra quasiparticle.

Thus we believe that the common feature associated with pairing in the n -leg t - J ladders is the formation of domain walls containing $d_{x^2-y^2}$ correlated pairs of holes. On the two-leg ladder, these domain walls appear simply as rung pairs. On the 4-leg ladder at a doping where the proximity effect response $\langle \Delta_d \rangle$ shown in Fig. 11 is large, one clearly sees the formation of four-hole domain walls composed of fluctuating $d_{x^2-y^2}$ pairs [8]. In the present 3-leg system, the domain wall structures form at higher doping levels and it is in this doping regime that pairing correlations appear.

We would like to thank L. Balents, M.P.A. Fisher, S.A. Kivelson, and T.M. Rice for useful discussions. SRW acknowledges support from the NSF under Grant No. DMR-9509945, and DJS acknowledges support from the NSF under grant numbers PHY-9407194 and DMR-9527304.

REFERENCES

- [1] K. Ishida, et. al., Phys. Rev. B **53**, 2827 (1996) and references therein.
- [2] M. Sigrist, T.M. Rice, and F.C. Zhang, Phys. Rev. B **49**, 12058 (1994).
- [3] S.R. White, R.M. Noack, and D.J. Scalapino, Phys. Rev. Lett. **73**, 886 (1994).
- [4] M. Azuma *et al.*, Phys. Rev. Lett. **73** 3463 (1994).
- [5] R.M. Noack, and D.J. Scalapino, and S.R. White, *Phil. Mag. B* **74**, 485 (1996).
- [6] M. Troyer, H. Tsunetsugu, and T. M. Rice Phys. Rev. B **53**, 251 (1996).
- [7] L. Balents and M.P. Fisher, Phys. Rev. B **53**, 12133 (1996).
- [8] S.R. White and D.J. Scalapino, to appear in PRB (cond-mat/9608138).
- [9] S.R. White, Phys. Rev. Lett. **69**, 2863 (1992), Phys. Rev. B **48**, 10345 (1993).
- [10] S.R. White, Phys. Rev. Lett. **77**, 3633 (1996).
- [11] S.R. White and D.J. Scalapino, Phys. Rev. B **55**, 6504 (1997).
- [12] N. Bulut and D.J. Scalapino, unpublished.
- [13] E. Arrigoni, *Phys. Lett. A* **215**, 91 (1996).
- [14] T. Kimura, K. Kuroki, and H. Aoki, Phys. Rev. B **54**, R9608 (1996).
- [15] H.-H. Lin, L. Balents, and M.P.A. Fisher, (cond-mat/9703055).
- [16] T. M. Rice, S. Haas, M. Sigrist, and F. Zhang, cond-mat/9706147.
- [17] S.A. Kivelson and V.J. Emery, p. 619 in *Proc. “Strongly Correlated Electronic Materials: The Los Alamos Symposium 1993,”* K.S. Bedell *et al*, eds. (Addison Wesley, Redwood City, Ca., 1994); V.J. Emery, S.A. Kivelson, and O. Zachar, preprint (cond-mat/9610094).

FIGURES

FIG. 1. Maximum likelihood hole configurations at various densities. In each case, the diameter of the black dots shows the probability of finding the last hole in the system at each site when all the other holes have been projected out in their most likely configuration, which is indicated by the gray dots.

FIG. 2. Spin configurations surrounding a domain wall. (a) For a 7×3 system with three holes, the width of the lines indicates the magnitude of $\langle \vec{S}_i \cdot \vec{S}_j \rangle$ between various sites when all three holes have been projected onto one of their most likely configurations. (b) For the same 7×3 system but with a staggered field applied at the left end, the length of the arrows indicates $\langle S_i^z \rangle$ when all three holes have been projected onto one of their most likely configurations.

FIG. 3. Hole density and spin moments showing domain walls. The diameter of the gray holes is proportional to the hole density $1 - \langle n_i \rangle$, and the length of the arrows is proportional to $\langle S_i^z \rangle$, according to the scales shown. (a) A 12×3 system with six holes, with a staggered field applied at the left end. (b) A 16×3 system with eight holes, with a staggered field applied along the bottom leg.

FIG. 4. Hole rung density for three different densities, on a 32×3 system. From bottom to top, the curves show four, twelve, and eighteen holes, corresponding to $x = 0.042$, $x = 0.125$, and $x = 0.1875$.

FIG. 5. $n(k) \equiv \langle \psi_0 | n_{k_x, k_y, s} | \psi_0 \rangle$ for a three leg ladder and a single chain. (a) A 32×3 system with $x = 0.042$. (b) A single chain system with $x = 0.1$. In each case, in order to reduce the effects of open boundary conditions, an average over many different $\langle \psi_0 | c_{i_x, i_y, s}^\dagger c_{j_x, j_y, s} | \psi_0 \rangle$ with the same separation $(j_x - i_x, j_y - i_y)$ was performed before Fourier transforming to get $n(k)$. Also, a smooth windowing function was applied to remove “ringing” near the Fermi surface.

FIG. 6. Same as Fig. 5, for higher densities.

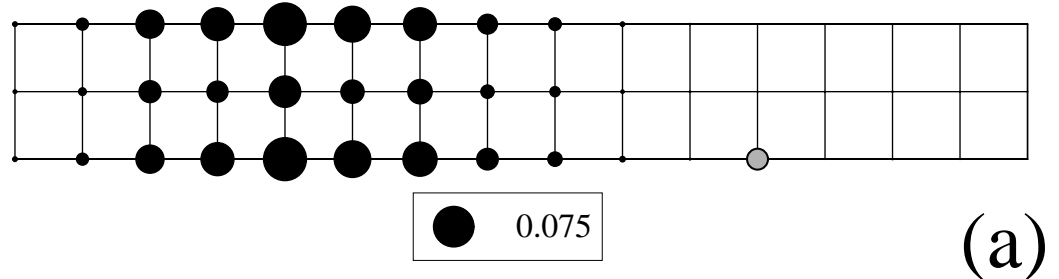
FIG. 7. Spin-spin correlations for two different densities on a 48×3 system. (a) A density of $x = 0.042$, showing power-law decay of the spin-spin correlations. (b) A density of $x = 0.125$, showing exponential decay of the spin-spin correlations. In each case, many different pairs of points are plotted simultaneously as a function of their separation, corresponding to different legs for each point as well as translations of pairs of points.

FIG. 8. Spin gap for a 44×3 system as a function of doping x .

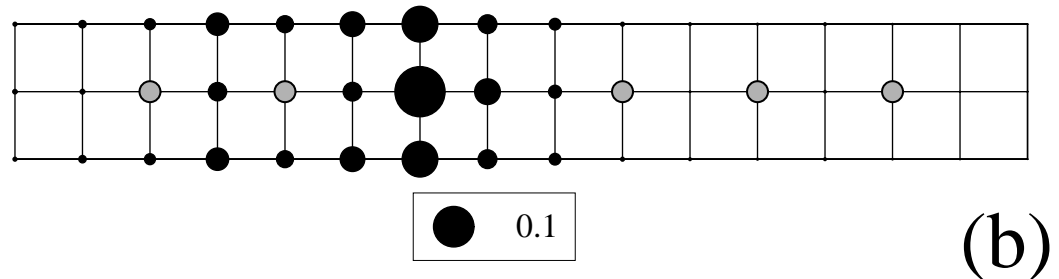
FIG. 9. Various measurements of pairing. In (a), the off-diagonal matrix element of $c_{i,\uparrow}c_{j,\downarrow}$ between the ground states of a 7×3 system with one hole and three holes is shown. The site i is fixed at the site $(4, 2)$, and the diameter of the gray dots shows the magnitude of the matrix element as a function of j . The sign of the matrix element is also indicated for each site. (b) The $d_{x^2-y^2}$ pairing correlation $D(l)$ is shown for three different densities, calculated on 32×3 ($x = 0.1875$) and 48×3 ($x = 0.04$, $x = 0.125$) systems. (c) The same data as in (b) for $x = 0.125$ plotted on a semi-log scale.

FIG. 10. $d_{x^2-y^2}$ pairing response to a proximity effect pair field operator for a single chain, and two, three, and four leg ladders. For the single chain, near-neighbor pairing is measured.

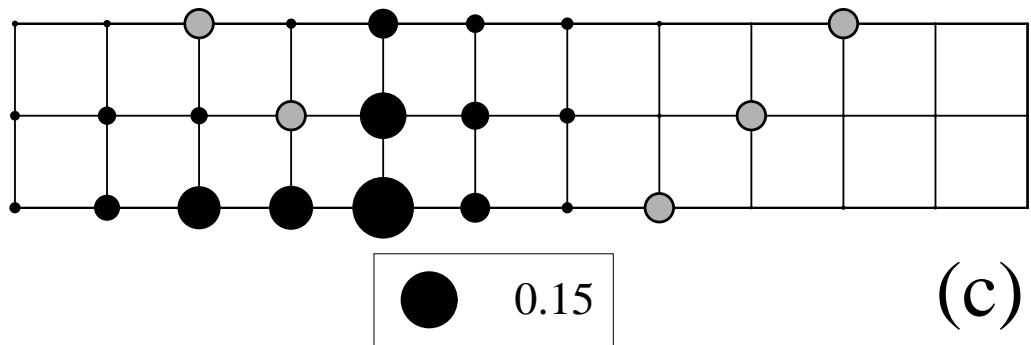
FIG. 11. Typical hole configurations in the transverse domain wall regime. Results for both (a) and (b) are from a 12×3 system with six holes, as in Fig. 1(c). (a) Typical hole configurations for all six holes sampled randomly, using a classical Monte Carlo procedure with probabilities measured with DMRG. (b) Typical hole configurations giving rise to $d_{x^2-y^2}$ pairing correlations. The positions of four holes are shown by black dots when the other two holes are “fluctuating” between the positions shown by gray dots.



16 x 3 system
 $J/t = 0.35$, 2 holes

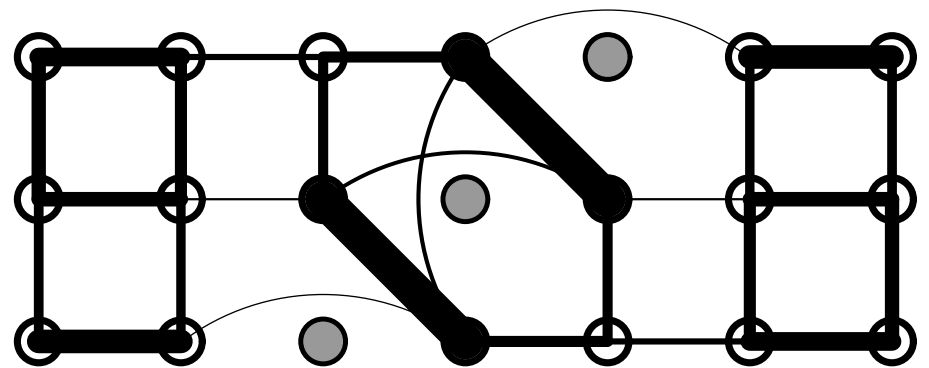


16 x 3 system
 $J/t = 0.35$, 6 holes

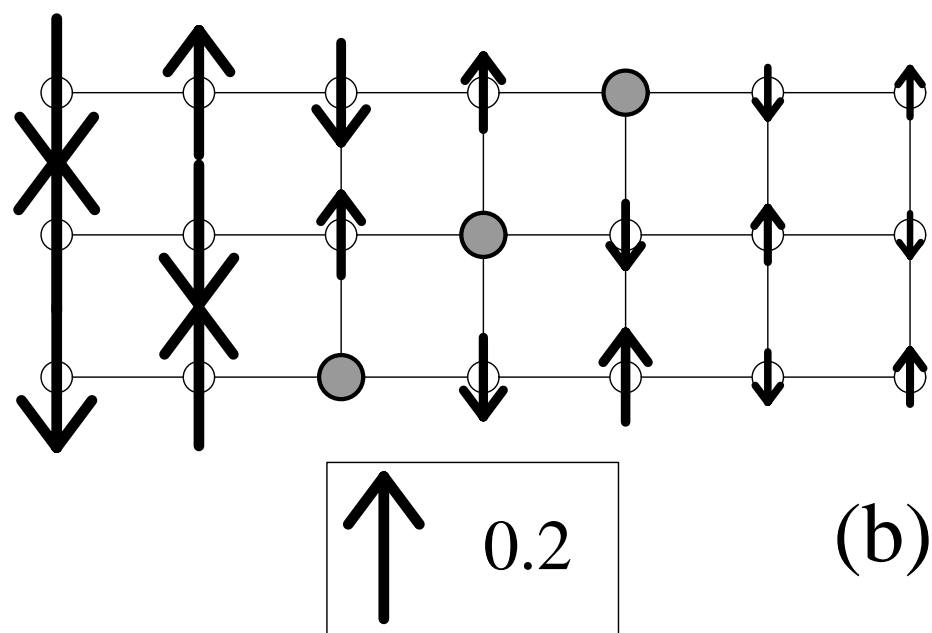


12 x 3 system
 $J/t = 0.35$, 6 holes

Fig. 1
 White and Scalapino

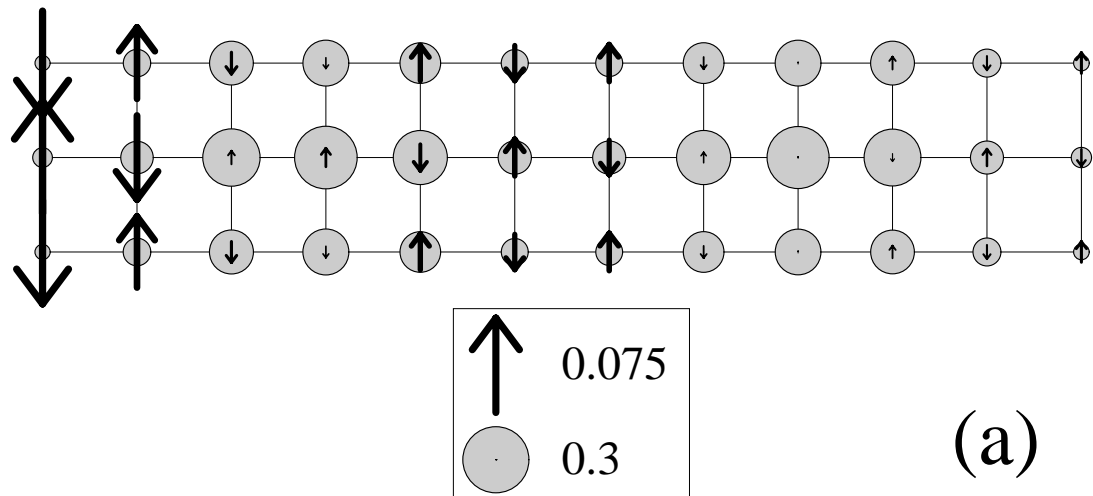


(a)

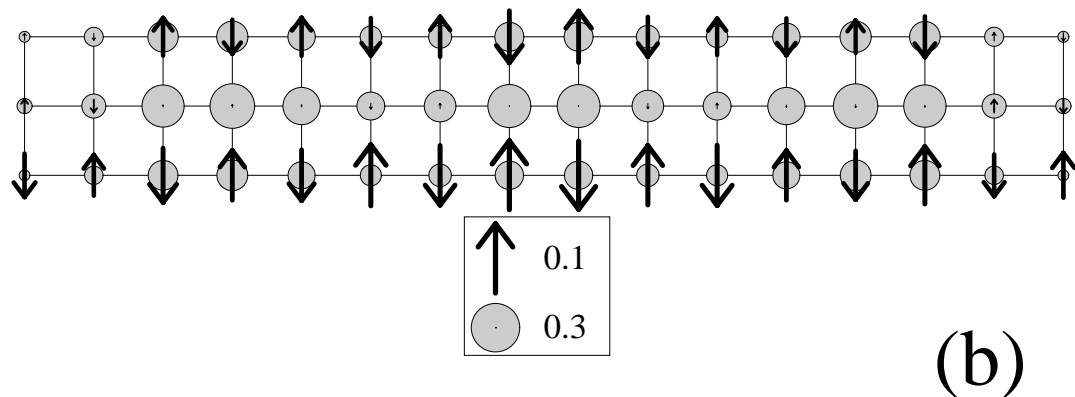


(b)

Fig. 2
White and Scalapino



12 x 3 system
 $J/t = 0.35$, 6 holes



16 x 3 system
 $J/t = 0.35$, 8 holes

Fig. 3
 White and Scalapino

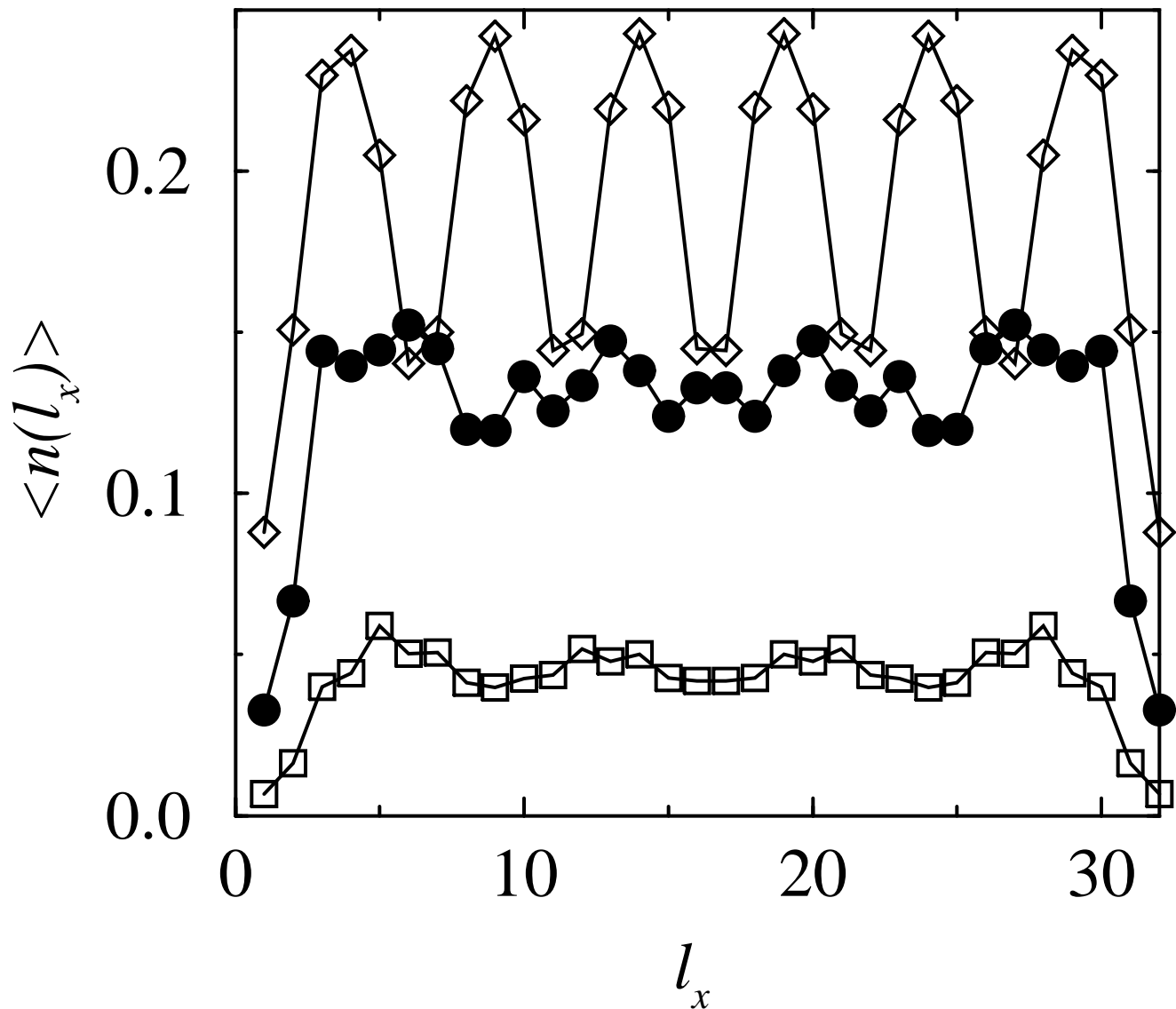


Fig. 4
White and Scalapino

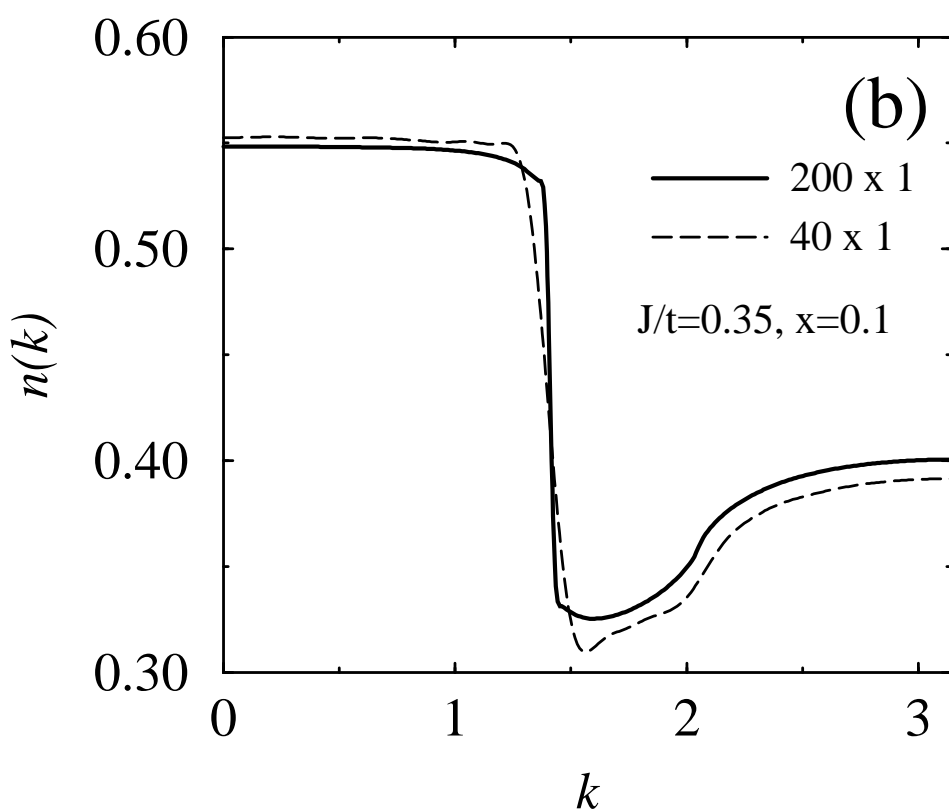
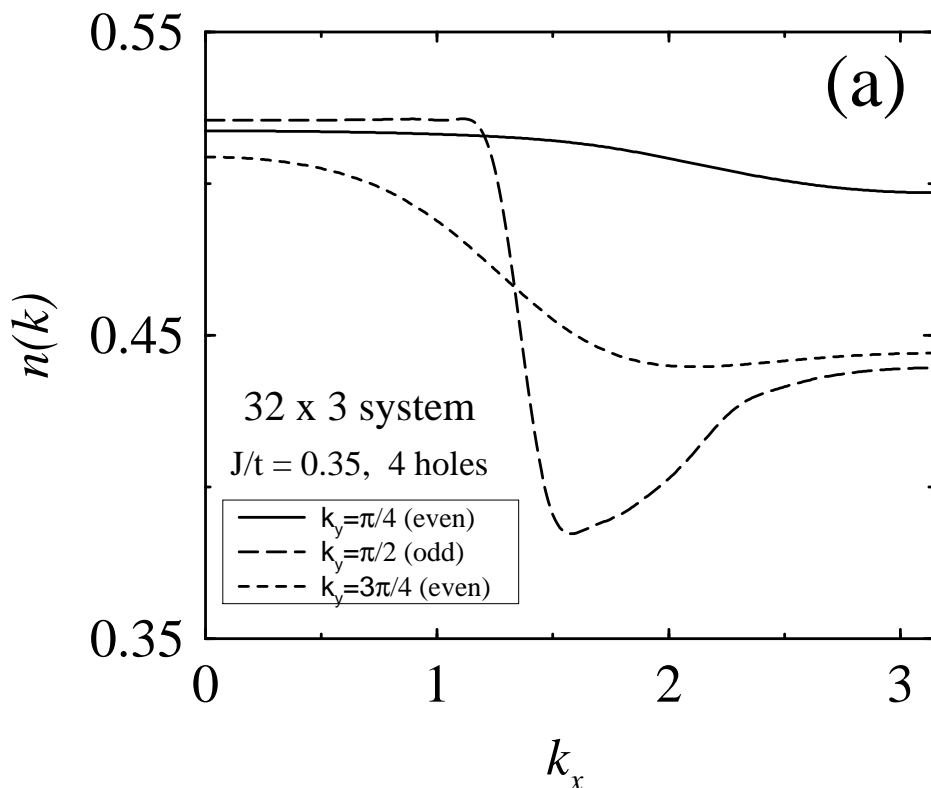


Fig. 5
White and Scalapino

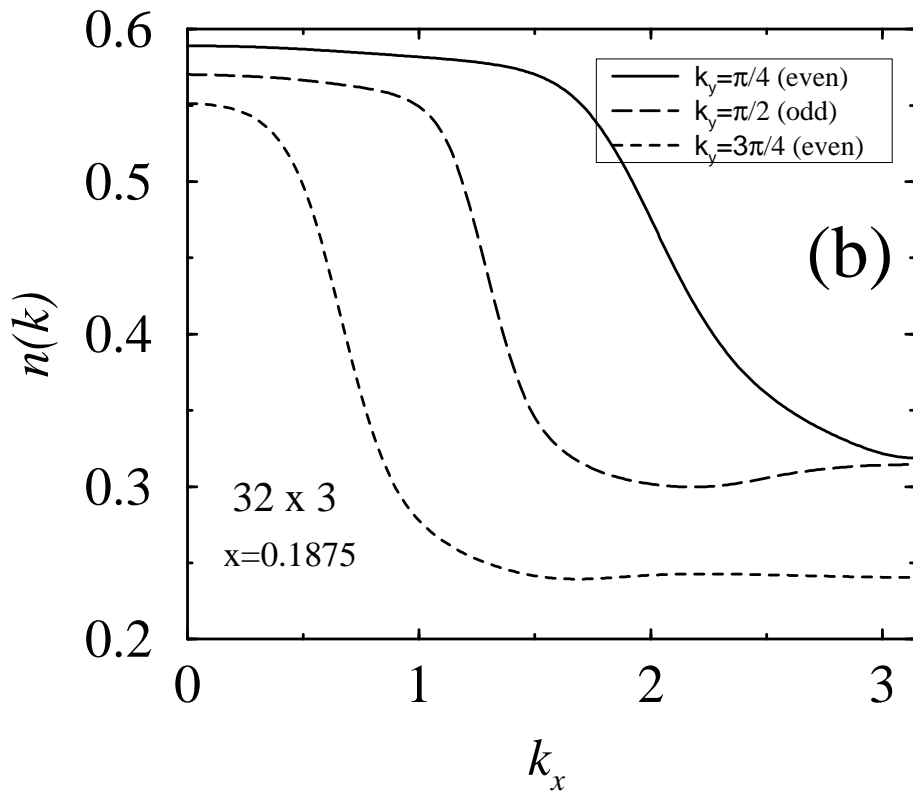
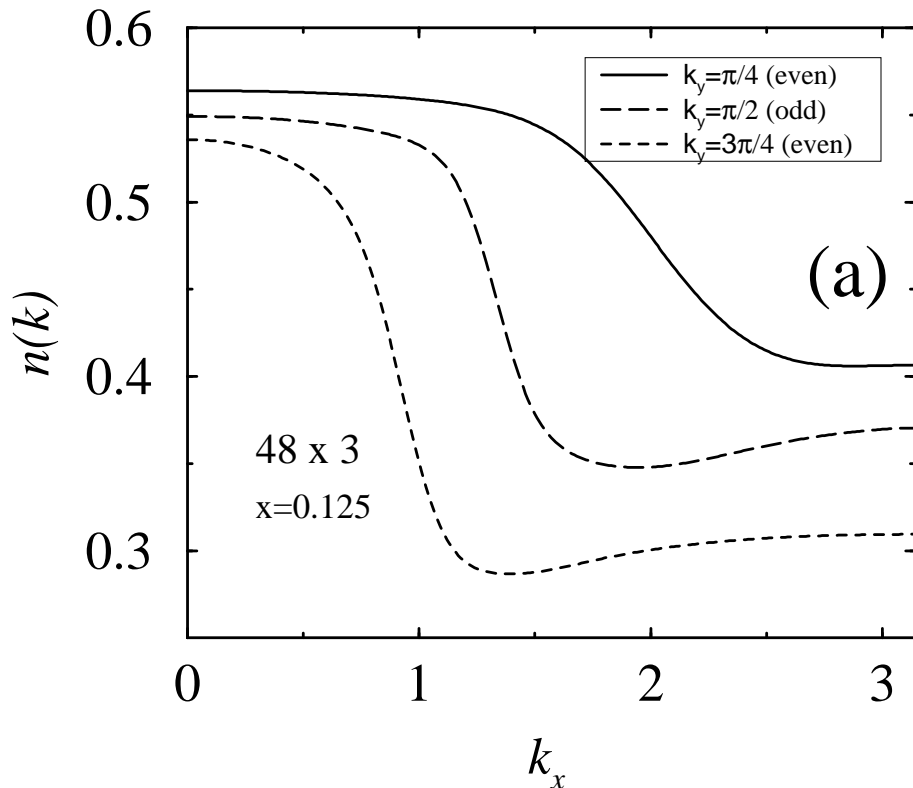


Fig. 6
White and Scalapino

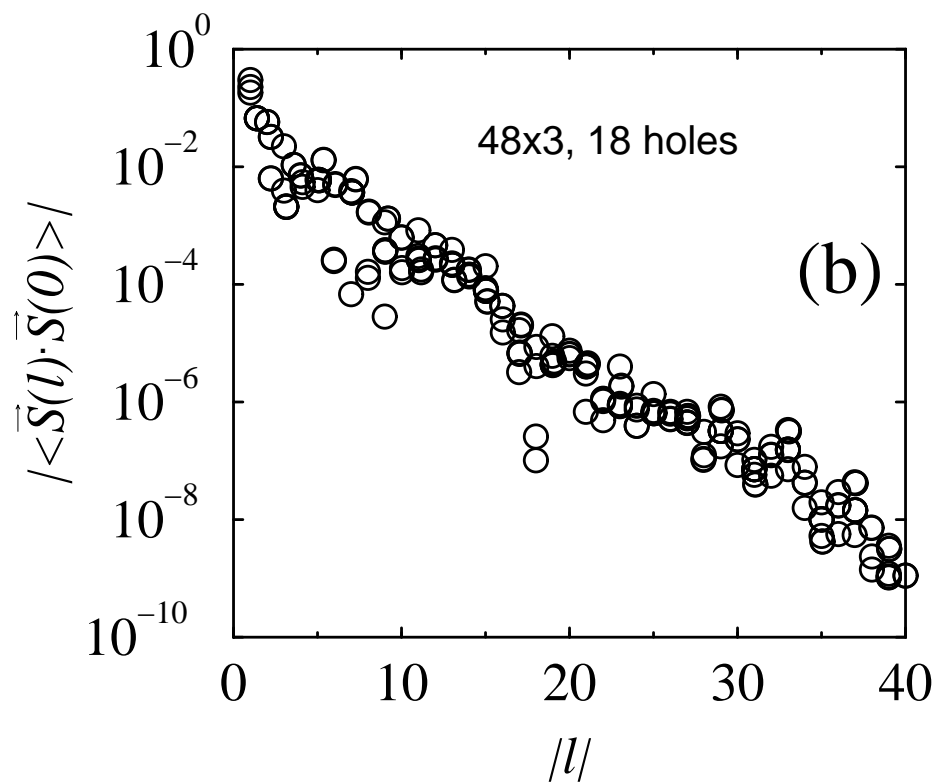
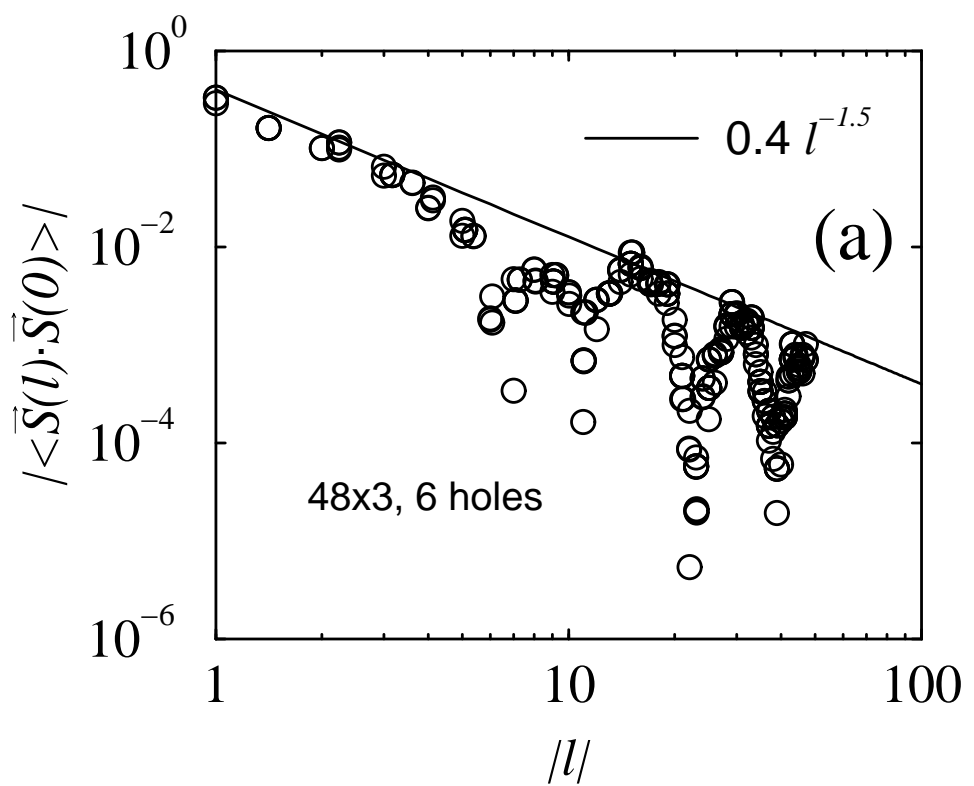


Fig. 7
White and Scalapino

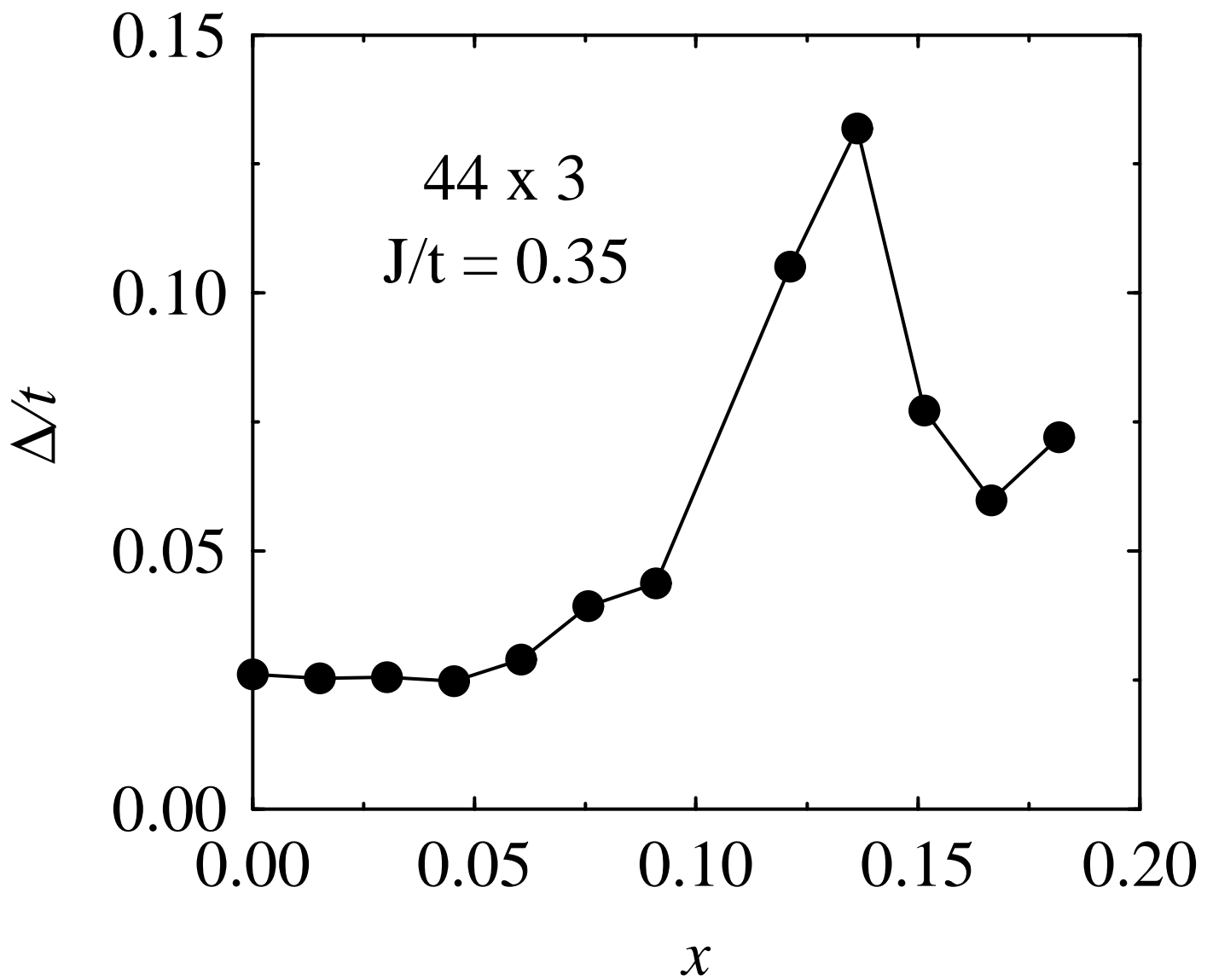
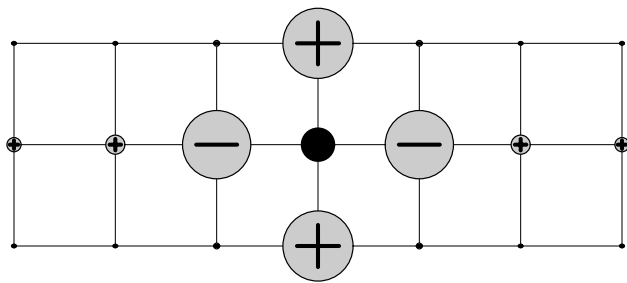
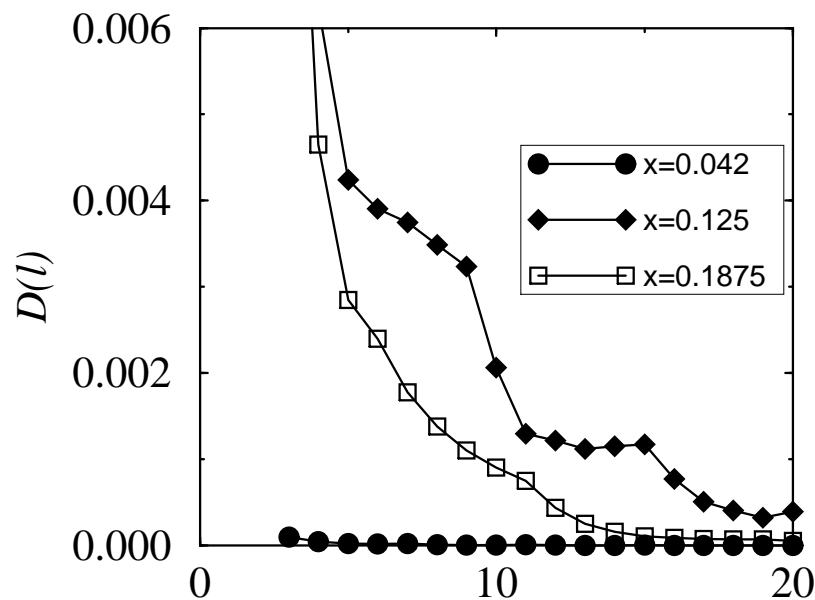


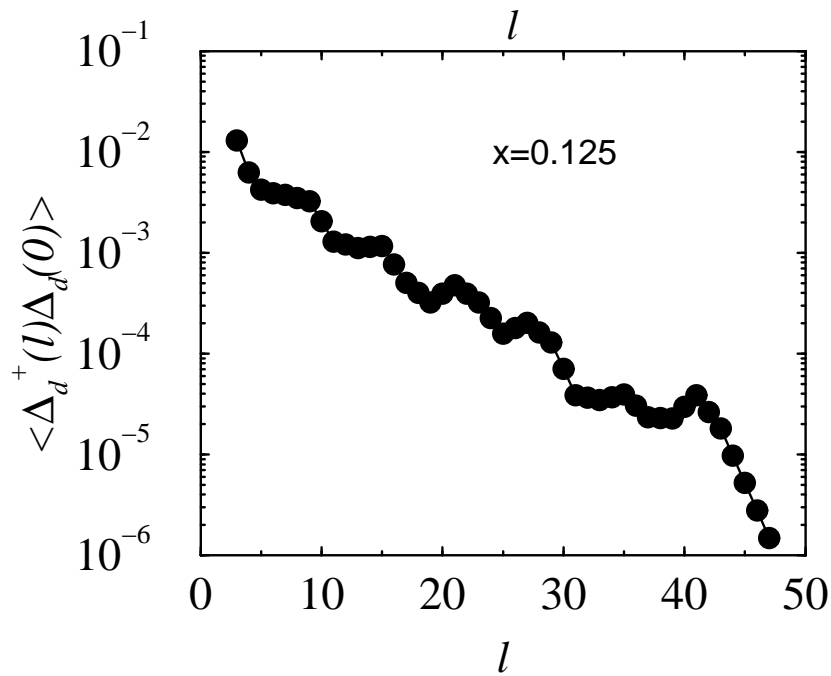
Fig. 8
White and Scalapino



(a)



(b)



(c)

Fig. 9
White and Scalapino

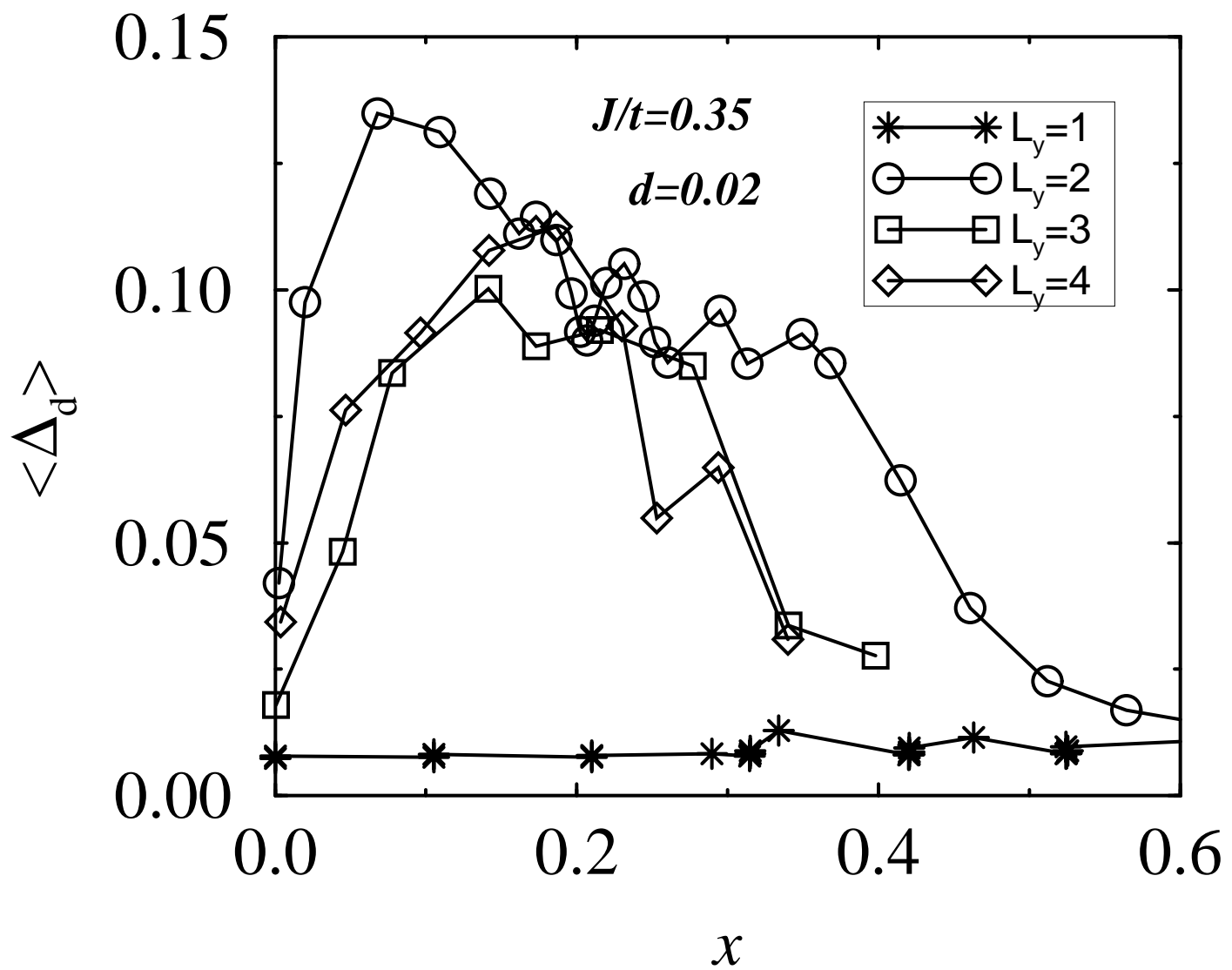
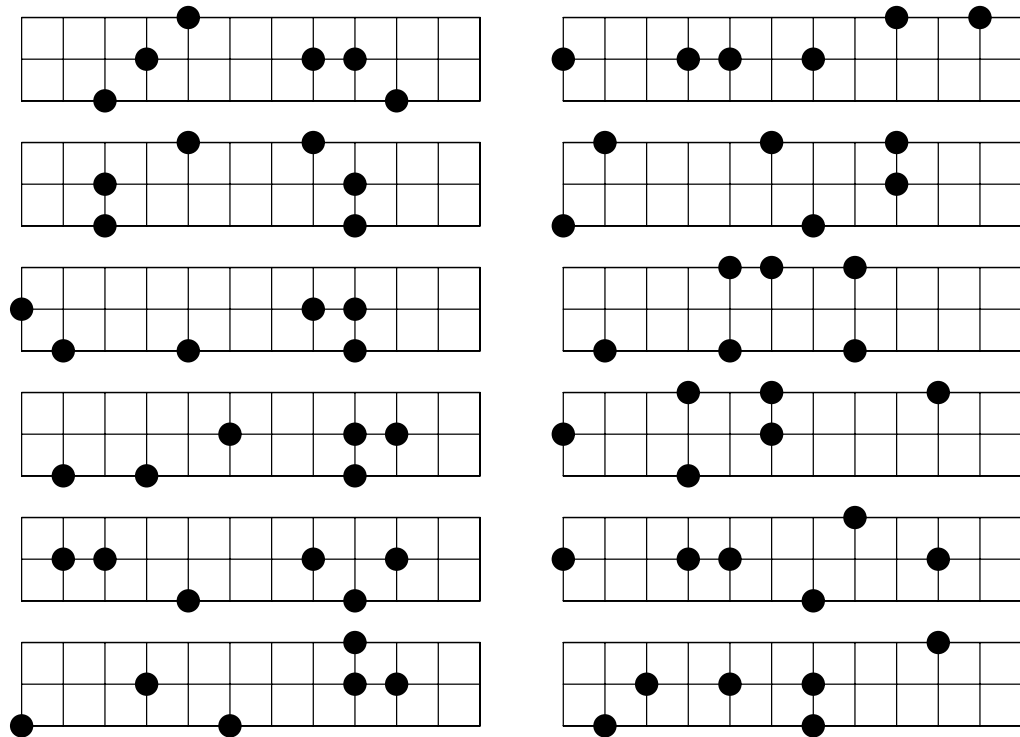
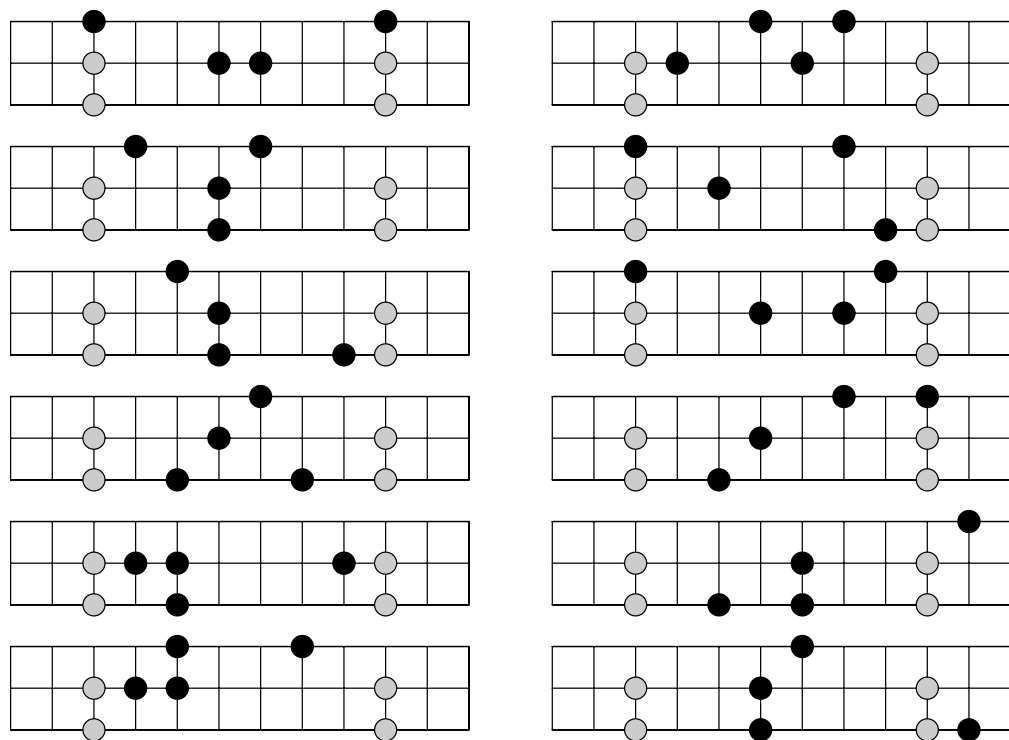


Fig. 10
 White and Scalapino



(a)



(b)

Fig. 11
White and Scalapino